Published in final edited form as:

Phys Med Biol. ; 64(11): 115022. doi:10.1088/1361-6560/ab1a44.

Ultrasound multiple scattering with microbubbles can differentiate between tumor and healthy tissue *in vivo*

Kaustav Mohanty[1], **Virginie Papadopoulou**[2], **Isabel G Newsome**[2], **Sarah Shelton**[2], **Paul A Dayton**[2], **Marie Muller**[1,3]

[1]Department of Mechanical and Aerospace Engineering, NC State University, Raleigh, NC 27695, United States of America

[2]UNC—NCSU Joint Department of Biomedical Engineering, UNC Chapel Hill, Chapel Hill, NC 27599, United States of America

Abstract

Most solid tumors are characterized by highly dense, isotropic vessel networks. Characterization of such features has shown promise for early cancer diagnosis. Ultrasound diffusion has been used to characterize the micro-architecture of complex media, such as bone and the lungs. In this work, we examine a non-invasive diffusion-based ultrasound technique to assess neo-vascularization. Because the diffusion constant reflects the density of scatterers in heterogeneous media, we hypothesize that by injecting microbubbles into the vasculature, ultrasound diffusivity can reflect vascular density (VD), thus differentiating the microvascular patterns between tumors and healthy tissue. The diffusion constant and its anisotropy are shown to be significantly different between fibrosarcoma tumors ($n = 16$) and control tissue ($n = 18$) in a rat animal model *in vivo*. The diffusion constant values for control and tumor were found to be 1.38 ± 0.51 mm^2 μs^{-1} and 0.65 ± 0.27 mm^2 μs^{-1}, respectively. These results are corroborated with VD from acoustic angiography (AA) data, confirming increased vessel density in tumors compared to controls. The diffusion constant offers a promising way to quantitatively assess vascular networks when combined with contrast agents, which may allow early tumor detection and characterization.

Keywords

multiple scattering; ultrasound imaging; diffusion constant; fibrosarcoma; contrast enhanced ultrasound; microbubbles

[3]Author to whom any correspondence should be addressed. mmuller2@ncsu.edu.

Conflict of interest

MM and PAD declare that they are inventors on a patent describing the diffusion constant based microvascular evaluation technique. Furthermore, PAD is an inventor on a patent describing AA and a co-founder of SonoVol, Inc., which has licensed this patent.

Data availability

Data supporting the findings presented in this manuscript are available from the corresponding author upon request.

Introduction

In this paper, we propose an ultrasound-based technology for the diagnosis and monitoring of cancer. This innovative technique assesses tumor-related angiogenesis in a non-invasive and quantitative manner. Angiogenesis is the formation of new blood vessels from pre-existing vessels and plays an important role in cancer. In tumors, angiogenesis has been established as one of the hallmarks of malignant transformation (Carmeliet 2005). Solid tumors need to recruit new blood vessels to grow beyond a certain size or for the hematogenous mode of metastasis (Folkman *et al* 1963). The morphology of such vessels resulting from tumor-related angiogenesis is abnormal. Unlike vasculature in healthy tissue, tumor vasculature is highly disorganized and isotropic (Jain 2014, Jain *et al* 2014). The vessels are tortuous with excessive branching and shunts (Carmeliet and Jain 2000). The microstructural properties of vascular networks, including micro-vessel density (MVD) and anisotropy are extremely relevant for distinguishing healthy tissue from multiple types of tumors (Eberhard *et al* 2000, Carmeliet 2005, Nico *et al* 2008). Various studies have linked MVD and vascular anisotropy to malignancy and overall prognosis (Weidner *et al* 1992, Gasparini *et al* 1994, Li *et al* 2000, Concato *et al* 2007, Al Murri *et al* 2008). MVD is commonly assessed via histopathology and has proven to be a significant and independent prognostic indicator (Weidner *et al* 1991, 1992).

Biopsy is the current gold standard for the diagnosis of malignancy. However, although biopsy is highly specific, it is invasive in nature and is subject to selection bias (Van Der Bij *et al* 2011). Thus, there is a significant interest in developing non-invasive, reliable methods to characterize the angiogenic microvasculature as a surrogate marker of malignancy. Various techniques, including ultrasound, micro-CT (Ehling *et al* 2014) and optical frequency domain imaging (OFDI) (Snoeks *et al* 2010), have been tested to characterize the microvasculature. Micro-CT scanning requires exposure to high intensity x-ray radiation in large doses, making it unsuitable for clinical use to visualize or monitor microvasculature. Optical coherence tomography (OCT) can be used to visualize the vasculature with a very good spatial resolution (typically 1–20 micron) but suffers from insufficient penetration depth (2 mm) (Fujimoto *et al* 2000, Vakoc *et al* 2012), (Yun *et al* 2003). Advanced OCT technologies, such as OFDI, can increase the acquisition speed, but penetration depth is still limited (4 mm) compared to ultrasound and micro-CT (Yun *et al* 2003). Micro-MRI imaging has shown some potential in high resolution imaging of the vasculature, but suffers from very large data acquisition time when micro resolution has to be achieved on large specimen (Uffen *et al* 2008).

Ultrasound is non-invasive and inexpensive compared to micro-CT and micro-MRI. Ultrasound imaging does not require any exposure to ionizing radiation, unlike micro-CT, and has much higher tissue penetration depth than OCT. However, the conventional ultrasonic imaging methods for cancer diagnosis lack specificity (Lixia *et al* 2016). To address this issue, methods relying on the use of ultrasound contrast agents have been developed for imaging the microvasculature (Sirsi *et al* 2012, Maresca *et al* 2014, Chong *et al* 2018). Current contrast agents for ultrasound are microbubbles, comprising a heavy molecular weight gas (typically a perfluorocarbon) encapsulated in a lipid shell to prolong lifetime in the circulation. The size of these agents, 1–8 μm in diameter, ensures that they act

as a blood marker, since they remain confined in the vasculature. Their unique behavior under ultrasound exposure allows preferential visualization of contrast signal using non-linear imaging techniques (Simpson *et al* 1999, Phillips 2001). The use of contrast-enhanced ultrasound for characterization of lesions, in the kidney (Setola *et al* 2007), prostate (Fillon 2013), breast (Sirsi *et al* 2012, Maresca *et al* 2014), sentinel lymph nodes in breast cancer (Sever *et al* 2011), and pancreas (D'Onofrio *et al* 2012), has been demonstrated clinically with varying degrees of success. Acoustic angiography (AA) is a novel contrast-enhanced ultrasound imaging technique relying on superharmonic imaging of microbubbles that enables the 3D mapping of micro-vascular networks with a resolution of 100–200 microns (Gessner *et al* 2013, Lindsey *et al* 2014, Shelton *et al* 2015, 2016). In preclinical studies, it has been shown that AA is able to differentiate tumors as small as 2–3 mm from healthy tissue (Shelton *et al* 2015), differentiate different tumor types based on their vascularity (Dunleavey *et al* 2014), and detect earlier response to radiation therapy (Kasoji *et al* 2018). Further clinical translation for the characterization of breast lesions is ongoing (Shelton *et al* 2017). However, AA does not directly provide quantitative information on the micro-architecture of vascular networks, which has to be obtained via intensive offline image processing.

In the present paper, we propose an ultrasound contrast technique exploiting the diffusive properties of microbubbles circulating in angiogenic networks, to quantify the density and anisotropy of vessels. The diffusivity of ultrasound waves in a heterogeneous medium is related to the scattering power of the scatterers, as well as the density of scatterers. The diffusion constant (D) indicates the rate at which the wave diffusive halo grows in the diffusive regime. We hypothesize that measuring the diffusion constant in vessels populated with microbubbles enables the quantification of vessel density. Numerous studies have recently been conducted, quantifying parameters related to the diffusivity, such as the diffusion constant and transport mean free path, to characterize the micro-architecture of heterogeneous media (Tourin *et al* 2000, Derode *et al* 2005, Aubry and Derode 2007, 2011, Aubry *et al* 2008). In particular, this has been successfully exploited in bone and the lung (Du *et al* 2017, Mohanty *et al* 2017), which are both highly scattering media with highly porous structures. This makes them ideal environments for architectural quantification using diffusion parameters, an approach previously explored by Page *et al* (1997, 1999) and Zhang *et al* (1999) and further advanced by Aubry *et al* (Aubry and Derode 2007). It was observed that the diffusion constant was significantly different between control and edematous (fluid-filled) lungs, enabling differentiation of the two tissues (Mohanty *et al* 2017). This difference in diffusivity was attributed to the reduced air content of lungs in rats suffering from edema, leading to reduced scatterer density. The diffusion constant has also been used to quantify trabecular bone density and structural anisotropy (Du *et al* 2017).

In the present study, microbubbles are used as scatterers. Due to multiple scattering by the microbubbles, the wave travels longer and more complex paths in the vessel network. This negatively affects imaging, but is an opportunity for the wave to extract additional information from the structure. In conventional ultrasound imaging, these multiple scattered signals are commonly treated as aberration or noise. We propose to exploit them instead, to obtain quantitative information on the microstructure of angiogenesis. By isolating the

incoherent contribution to the backscattered intensity, it is possible to measure the diffusion constant, which is an indicator of the density of scatterers.

We demonstrate that the diffusion constant in microbubble populations, can be used to characterize the density and anisotropy of vascular networks. In a rodent study *in vivo*, we show that there are significant differences in the diffusion constant measured in fibrosarcoma tumors *(N* = 16) versus in the healthy tissue in the contralateral flank of the animals (*N* = 18). To quantify the anisotropy, we measure the diffusion constant along two perpendicular orientations of transducer placement on each rat.

Methodology

Materials

Microbubble contrast agent preparation—Microbubble contrast agents were prepared following a previously published protocol (Shelton *et al* 2015) by combining 1,2-distearoyl-sn-glycero-3-phosphocholine (DSPC) and 1,2-distearoyl-sn-glycero-3-phosphoethanolamine-N-[methoxy (polyethylene glycol)2000] (DSPE-PEG2000) (Avanti Polar Lipids; Alabaster, AL, USA) in a 9:1 molar ratio. Lipids were dissolved in phosphate-buffered saline containing 15% (v/v) propylene glycol and 5% (v/v) glycerol for a final lipid concentration of 1.0 mg ml^{-1}. 1.5 ml aliquots of the resulting solution were then added to 3 ml glass vials. The air in the headspace of each vial was then exchanged with decafluorobutane (DFB) gas (FluoroMed; Round Rock, TX, USA). Microbubbles were formed by 45 s of mechanical agitation in a Vialmix (Lantheus Medical Imaging; North Billerica, MA, USA).

In vivo experiments—A total of 18 Female Fischer-344 rats (Charles River Laboratories, Inc.; Wilmington, MA, USA) were used in this study (approx. 180 g, 12–16 weeks old). The animals were handled according to National Institute of Health guidelines, and the study protocol was approved by the UNC Institutional Animal Care and Use Committee. Fibrosarcoma tumors were grown in the right flank of 16 animals after subcutaneous implantation of 1 mm^3 tumor tissue sections from donor animals (Fix *et al* 2017). The left flank of all 16 animals was used as control. Two more animals, in which no tumor was implanted were also used as control.

The animals were anesthetized in an induction chamber with 5% vaporized isoflurane. A 24-gauge catheter was inserted into the animal's tail vein for the administration of the contrast agent solution. The animal's right flank (tumor side) and the contralateral control side were shaved, and ultrasound gel was placed between the transducer and the animal's skin to ensure proper coupling during data acquisition. During data acquisition, the animals were placed on a heating pad, and isoflurane was maintained at 2%−2.5%. Each animal was first scanned with the Verasonics Vantage scanner to obtain the IRM for diffusivity assessment and then transferred to a Vevo 770 for B-mode and AA imaging. The size of the tumor at the time of data acquisition was estimated using the Vevo770 B-mode scanner (see Data Acquisition).

The microbubble solution was diluted with sterile saline in a ratio of 1:10 (10^9 bubbles ml^{-1}) and 1:1 for the measurement of *D* and AA, respectively. The diluted microbubble solution was infused through the tail vein of each animal at a rate of 30 μl min^{-1} using an infusion pump connected to a syringe (PHD 2000, Harvard Apparatus, Cambridge, MA,USA) (Gessner *et al* 2012) during data acquisition. We estimate the microbubble concentration to be around 5×10^7. microbubbles ml^{-1} for the *in vivo* experiments, assuming blood volume in an average rat to be approximately 20 ml for female and 30 ml for male (Lee and Blaufox 1985). It should be noted that the microbubbles were not continuously mixed in the syringe, which might have reduced the supplied bubbles. Multiple scattering acquisitions were acquired with a L11–4v transducer, placed in two perpendicular orientations (transverse and coronal) across the tumor on tumor-bearing sides ($n = 16$), as shown on figure 1(A). Control data was also acquired in two orientations on the contralateral control side, and on animals without tumors ($n = 18$). Measurements on the tumor-free, control flanks were obtained in the same anatomical region as the tumor implants. We ensured that these two planes approximately passed through the center of the tumor (largest cross-section) using B-mode imaging. Then, AA scans of both the tumor and contralateral sides were acquired as described below in the Data Acquisition section.

Data acquisition

Inter-element response matrix (IRM)—A Verasonics L11–4v linear array transducer connected to a Verasonics 128 Vantage scanner (Verasonics, Inc.; Kirkland, WA, USA) operating at 7.8 MHz was used to acquire the IRM. The IRM is a 3D matrix containing the backscattered signals recorded over the entire array for signals transmitted consecutively by individual elements of the array (Aubry and Derode 2007, 2011, Aubry *et al* 2008, Du *et al* 2017, Mohanty *et al* 2017). All 128 elements of the array were sequentially used to transmit a two cycle Gaussian pulse with peak-to-peak pressure equal to 300 kPa. For each transmit event, all 128 elements recorded backscattered echoes simultaneously for 50 μs. The IRM was recorded using a samplingfrequency of 62.5 MHz. The acquired IRM has dimensions128 × 128 × 3125, where 3125 is the number of time points.

Acoustic angiography (AA)—Volumetric B-mode and acoustic angiography (AA) images were acquired on a Vevo 770 scanner (VisualSonics; Toronto, ON, CA) by translating the probe in one dimension, as shown in figure 1(B). Tumor volume was calculated from B-mode as the ellipsoidal volume from sagittal and transverse planes of the largest tumor crosssection. AA was successfully acquired for 13/18 control and 14/16 tumor-bearing rats (due to our protocol's cumulative anesthesia time constraint or probe unavailability at the end of the study, data was not acquired for all animals) using a modified 30 MHz single-element transducer (RMV 707, VisualSonics; Toronto, ON, CA) to which an added confocal 4 MHz annular element. Contrast images were acquired by transmitting with the low frequency element and receiving broadband superharmonic signals with the high frequency element during a continuous infusion of microbubbles, which were administered through the tail vein at a rate of 1.5×10^8 microbubbles min^{-1}. 3D images were acquired with a step size of 100 μm, averaging two frames in every location, at a frame rate of 4 frames per second (Gessner *et al* 2013, Shelton *et al* 2015, 2016). The 3D data was then resampled to a uniform step size of 50 μm to obtain isotropic voxels. Figure 2 displays

examples of sagittal maximum intensity projections (MIPs) for a control and tumor case, providing a 2D projection of the 3D volumetric data.

Data processing

Diffusion constant measurements—The IRM data acquired using the Verasonics was processed to extract the diffusion constant. A time shift was applied to all backscattered signals in the IRM along the time dimension such that the arrival of the first backscattered echo occurs at time $t = 0$ for all emitter–receiver pairs. This allowed to compensate for differences in emitter-receiver distances. Each time signal of the IRM (denoted as the matrix H) can be represented by $h_{ij}(t)$, where i is the emitter number and j the receiver number. The signal is then divided into overlapping time windows (each 0.5 js long with 50% overlap). The backscattered intensity $I_{ij}(T)$ is calculated over each time window, where T is the time at the center of the time window, and Δ. is the width of the time window. The width of the time window was chosen based on the central frequency, such that it spans over 1 to 2 wavelengths (Tourin *et al* 2000, Aubry and Derode 2007, Aubry *et al* 2008).

$$I_{ij}(T) = \int_{t_0(T)}^{t_0(T)+\Delta} h_{ij}^2(t)dt \tag{1}$$

The average backscattered intensity $I(r, T)$ .was calculated by averaging the backscattered intensity over transducer-receiver couples separated by the same distance ($r = |i - j| \times w$).. Here, w is the pitch of the transducer array ($w = 0.3$ mm). In order to separate the coherent and incoherent contributions to the intensity, the H matrix was transformed into an antisymmetric matrix M, such that

- $m_{ij} = h_{ij}$ for $i <$ j,
- $m_{ij} = -h_{ij}$ for $i > j$
- $m_{ij} = 0$ for $i = j$.

The backscattered intensity $I_{ij}^A(T)$. and the averaged backscattered intensity I^A. (r, T) was then calculated from the antisymmetric matrix following a similar procedure. The coherent $I_{coherent}(r, T)$. and incoherent $I_{incoherent}(r, T)$ .intensities were extracted by respectively adding or subtracting the intensities resulting from the matrices H and M (Aubry and Derode 2007).

$$I_{coherent}(r, T) = \frac{I(r, T) - I^A(r, T)}{2} \tag{2}$$

$$I_{incoherent}(r, T) = \frac{I(r, T) + I^A(r, T)}{2}. \tag{3}$$

In the diffusive regime, the incoherent intensity can be expressed as a function of the diffusion constant, D:

$$I_{inoherent}(r,T) = I(T) \times \exp\left(-\frac{r^2}{4DT}\right). \quad (4)$$

The diffusion constant was then calculated by fitting a Gaussian curve to the incoherent intensity $I_{inc}(r, T)$ for multiple consecutive time windows. The variance of these Gaussian curves is plotted against time and the slope of the linear trend enables us to calculate the D. An inclusion criteria of R-squared > 0.4 was set for obtaining the D. Once the D values were obtained for the two orientations of the probe, the anisotropy ratio was calculated by taking the ratio of D along the transverse plane and coronal planes.

Vascular density (VD)—The VD corresponding to the planes used in the IRM acquisitions was calculated from AA data. This was done by following the same method as in previously published work from AA post-processing (Dunleavey *et al* 2014, Shelton *et al* 2015, Kasoji *et al* 2018), for regions of the data corresponding to the IRM acquisitions. In order to extract sub-volumes of AA data approximately registered to the planes of IRM data, the coordinates of the center of the tumor on the sagittal plane were used to determine the center planes used in the coronal and transverse sub-volumes. Since the animal had to be repositioned between imaging systems and different transducers used, this gives an approximate matching and should not be interpreted as being the exact same planes as used for IRM. Regions of interest (ROIs) were defined for both the coronal and transverse planes acquired as illustrated in figure 1(A). The plane thickness for each sub-volume was taken as the elevational aperture of the L11–4v (5 mm) in order to mimic the slice thickness that would correspond to the IRM acquisitions. For each sub-volume ROI corresponding to the IRM acquisition planes, the VD was calculated as the ratio of voxels above the thresholding value chosen obtained using Otsu's method (Otsu 1979, Kasoji *et al* 2018), for regions of the data corresponding to the IRM acquisitions.

Data analysis and statistical methods—The diffusion constant was calculated from IRM acquisitions for both orientations in tumors and controls, and the anisotropy ratio was defined as the ratio of these values. Differences between D values obtained from control coronal plane, control transverse plane, tumor coronal plane, and tumor transverse plane were tested using the Kruskal–Wallis test with Dunn's post-test (data was not normally distributed, so non-parametric analysis was chosen). The anisotropy ratio was also compared between tumors and controls using a Wilcoxon–Mann–Whitney test (non-normal distribution).

To confirm the hypothesis that the VD (calculated from AA sub-volumes corresponding to the IRM acquisition slices) of tumors was higher than that of controls, in both coronal and transverse orientations, a one-tailed t-test was used after confirming normality with a Kolmogorov–Smirnov test.

All data are presented as mean ± standard deviation. Statistical significance was set *a priori* at $p < 0.05$ and is graphically depicted on all figures as (*) for $p < 0.05$, (**) for $p < 0.01$ and (***) for $p < 0.001$, as well as (NS) to denote non-statistically-significant comparisons.

Statistics were performed on GraphPad Prism version 5.01 (GraphPad Software; San Diego, California, USA).

Results

Diffusion constant and anisotropy ratio (*in vivo* experiments)

For the 16 tumor-bearing rats, the mean tumor diameter was 7.8 ± 3.4 mm, and the mean tumor volume was 360 ± 508 mm^3 (range 50.9 mm^3 to 2349.7 mm^3). The diffusion Constant is extracted from the time evolution of the backscattered intensity as described in the methodology section. The variance of the Gaussian fit is plotted with time as shown in figure 3. These plots of the variance time-evolution are fitted with a linear model to obtain the slope, which is equal to twice the Diffusion Constant. For the tumor case, it can be clearly seen that the variance grows much more slowly than in the control μm case.

Figure 4(A) shows the D values obtained for both orientations for control and tumor flanks ($n_{control}$ = 18; n_{tumor} = 16). Significant differences were observed for D values obtained in the transverse and coronal orientations for control regions (transverse: 1.61 ± 0.51 $mm^2\ \mu s^{-1}$, coronal: 1.05 ± 0.31 $mm^2\ \mu s^{-1}$, $p < 0.05$). However, for tumors, there was no significant difference along the two orientations (transverse: 0.67 ± 0.22 $mm^2\ \mu s^{-1}$, coronal: 0.61 ± 0.28 $mm^2\ \mu s^{-1}$, $p > 0.05$). The D values for control and tumor, combining both orientations, were found to be 1.38 ± 0.51 $mm^2\ \mu s^{-1}$ and 0.65 ± 0.27 $mm^2\ \mu s^{-1}$, respectively. The anisotropy ratio of control and tumor regions are compared in figure 4(B). The closer the anisotropy ratio is to one, the higher the isotropy of the tissue's vascular network. It is evident that control tissue exhibits significantly higher anisotropy ratios than tumor-bearing tissue, with ratios of 1.62 ± 0.91 versus 1.13 ± 0.51, respectively ($p < 0.05$).

Vascular density (VD)

In both the coronal and transverse slices corresponding to the IRM acquisitions, the VD obtained from AA were significantly higher in tumors (n = 14) compared to controls (n = 13), as shown in figure 5. The VD for control in the transverse and coronal plane was observed to be 4.82% ± 1.87% and 4.71% ± 1.96%. Whereas, the VD for tumor in the transverse and coronal plane was observed to be 7.21% ± 3.05% and 6.59% ± 3.04%.

Discussion

We have demonstrated that the nominal values of both the diffusion constant, D, and the anisotropy of D measured using ultrasound multiple scattering by microbubbles are significantly different between tumor-bearing and control tissue *in vivo*. For *in vivo* cases, D can indeed be thought of as an indirect measure of the microvascular density. When D is measured along two different orientations and compared, it has the ability to indicate the extent of vessel anisotropy.

From the diffusion constant values, we can deduce that the degree of isotropy is much higher in tumor-bearing tissue than in control tissue. This is expected, since normal vasculature is arranged in a hierarchy of evenly spaced, directional and well-differentiated arteries, arterioles, capillaries, venules and veins, whereas in tumor proliferation, angiogenesis leads

to multi-directional, chaotic and disorganized vasculature (Nagy *et al* 2009). Tumor-bearing tissue exhibits relatively low variability in diffusivity, and the anisotropy ratios obtained from diffusivity measurements were significantly higher in control tissue, depicting a preferred orientation of vessel growth. Comparisons between diffusion constant values and VD measurements from AA data (shown in figure 5) also support the hypothesis that diffusion constant measurements are reflective of the underlying VD of the tissue. Higher VD values for tumor-bearing tissue support the assumption that tumor vascular networks are indeed more random and have higher density.

Although the difference between the D Values for the two types of tissue (healthy and tumor) is significant, there is variability in the Diffusion Constants measured amongst individual rats is high, leading to relatively large error bars. Larger error bars are observed for control cases. This is probably due to the fact that very few vessels were captured in the healthy tissue. On the contrary, for tumor tissue, tighter error margins are observed, which may signify the homogeneity of tumor from rat to rat and within one rat for multiple readings.

The main limitation of the proposed approach is that it does not allow a local estimation of the diffusivity of the complex microbubble filled medium. The diffusion constant indicates the rate at which the wave diffuses in a scattering medium. By nature, it is a parameter that reflects multiple scattering events and diffusion through a region of interest larger than the wavelength. To obtain the Diffusion Constant, both spatial and time averaging need to be performed. Therefore, D is an quantitative parameter that reflects the vessel density of the region of interest on average. The tumor dimensions in the *in vivo* experiments (approx. <10 mm) are less than the length of the transducer (35 mm). Consequently, the D values measured in tumor tissue reflect a VD intermediate between the actual vessel density of tumor, and the vessel density of control tissue. Variations in tumor size might have negatively affected the value of D. for smaller tumors, the D values might have been underestimated, when averaged with values in neighboring healthy tissue. However, no correlation was found between D and tumor size. The diffusion constant for tumor cases still shows significant difference from control cases, even with this spatial averaging. This may mean that the actual diffusion constant for tumor cases would be lower when we do not account for non-tumor regions. In the future, one could combining the measurement of D to conventional ultrasound imaging and use a subset of ultrasound array elements in order to conduct localized measurement of D (Mohanty *et al* 2018). However, if too few elements are used, the number of points representing the incoherent backscattered intensity would be reduced, which might affect the accuracy of the Gaussian fits and a lead distorted linear variance trend. This will be the subject of future studies.

The wavelength chosen will influence the time window over which the time-dependent intensity is calculated (the time window is chosen to ensure that most windows contain a scattering event). The nonlinearity of the microbubbles is not fully exploited in the present work, but exploiting the harmonic response in the context of diffusion will be the focus of subsequent studies.

Super-resolution techniques allow imaging of angiogenic networks with outstanding spatial resolution (Errico *et al* 2015, Lin *et al* 2017). However, extracting quantitative parameters from these images requires heavy off-line post-processing. 3D ultrafast doppler tomography (UFD-T) has shown promise during preliminary studies (Alcázar 2006, Provost *et al* 2015) but acquisition times are currently too slow for clinical use and can take up to an hour. Although the present method does not achieve super-resolution, we propose it as an alternative that does not require any image processing, and can be used in near real-time, maybe in combination with conventional B-mode imaging, to improve the specificity of ultrasound for cancer diagnosis.

A great advantage of the measurement of the Diffusion Constant is that the information extracted is quantitative and is expected to correspond to the vessel density of individual animals. This will be tested in future studies. Combining images obtained with other contrast-enhanced imaging methods, such as AA or conventional B-mode ultrasound, with the diffusion constant and estimation of the anisotropy would provide a comprehensive set of data that has the potential to improve the specificity of ultrasound diagnosis. This combined approach could be used in the future for monitoring the response to anti-angiogenic treatments.

Conclusion

The use of microbubbles promotes multiple scattering. Multiple-scattered waves take long paths in the microstructure, and their complex backscattered signal contains information about the density and orientation of the vasculature. By extracting the incoherent backscattered contribution from the total backscattered intensity, it is possible to obtain the diffusion constant, which is a good metric of the diffusivity of the medium, i.e. the rate at which the incoherent contribution to the signal diffuses in a complex medium. In this study, we show that the diffusion constant enables the quantitatively characterization of blood vessel network, and is are related to vessel density. Significant differences are observed between control ($D = 1.38 \pm 0.51$ mm^2 μs^{-1}) and tumor-bearing ($D = 0.65 \pm 0.27$ mm^2 μs^{-1}) tissues. In addition to vessel density, the diffusion constant also allows characterize the existence of anisotropy in control blood vessels (1.62 ± 0.91) and confirm that tumor blood vessels (1.13 ± 0.51) are more isotropic. This approach could be utilized to non-invasively assess and quantify the microvasculature.

Acknowledgment

This project was partly funded by NIH R01CA170665, R44CA165621, R03EB022311 and R01CA189479. IG Newsome was supported in part by training program T32HL069768 and SE Shelton was supported by NIH F99CA212227.

References

Al Murri AM, Hilmy M, Bell J, Wilson C, McNicol AM, Lannigan A, Doughty JC and McMillan DC 2008 The relationship between the systemic inflammatory response, tumour proliferative activity, T-lymphocytic and macrophage infiltration, microvessel density and survival in patients with primary operable breast cancer Br. J. Cancer 99 1013–9 [PubMed: 18797461]

Alcázar JL 2006 Tumor angiogenesis assessed by three-dimensional power Doppler ultrasound in early, advanced and metastatic ovarian cancer: a preliminary study Ultrasound Obstet. Gynecol 28 325–9 [PubMed: 16906635]

Aubry A and Derode A 2007 Ultrasonic imaging of highly scattering media from local measurements of the diffusion constant: separation of coherent and incoherent intensities Phys. Rev. E 75 1–9

Aubry A and Derode A 2011 Multiple scattering of ultrasound in weakly inhomogeneous media: Application to human soft tissues J. Acoust. Soc. Am 129 225 [PubMed: 21303005]

Aubry A, Derode A and Padilla F 2008 Local measurements of the diffusion constant in multiple scattering media: application to human trabecular bone imaging J. Acoust. Soc. Am 123 3633

Carmeliet P 2005 Angiogenesis in life, disease and medicine Nature 438 932–6 [PubMed: 16355210]

Carmeliet P and Jain RK 2000 Angiogenesis in cancer and other diseases Nature 407 249–57 [PubMed: 11001068]

Chong WK, Papadopoulou V and Dayton PA 2018 Imaging with ultrasound contrast agents: current status and future Abdominal Radiology vol 43 (Berlin: Springer) pp 762–72 [PubMed: 29508011]

Concato J, Jain D, Li WW, Risch HA, Uchio EM and Wells CK 2007 Molecular markers and mortality in prostate cancer BJU Int 1001259–63

D'Onofrio M, Barbi E, Dietrich CF, Kitano M, Numata K, Sofuni A, Principe F, Gallotti A, Zamboni GA and Mucelli RP 2012 Pancreatic multicenter ultrasound study PAMUS) Eur. J. Radiol 81 630–8 [PubMed: 21466935]

Derode A, Mamou V, Padilla F, Jenson F and Laugier P 2005 Dynamic coherent backscattering in a heterogeneous absorbing medium: application to human trabecular bone characterization Appl. Phys. Lett 87 1–3

Du H, Mohanty K and Muller M 2017 Microstructural characterization of trabecular bone using ultrasonic backscattering and diffusion parameters J. Acoust. Soc. Am 141 EL445–51 [PubMed: 28599551]

Dunleavey JM. et al. 2014; Vascular channels formed by subpopulations of PECAM1 + melanoma cells. Nat. Commun. 5:5200. [PubMed: 25335460]

Eberhard A, Kahlert S, Goede V, Hemmerlein B, Plate KH and Augustin HG 2000 Heterogeneity of angiogenesis and blood vessel maturation in human tumors: implications for antiangiogenic tumor therapies Cancer Res 60 1388–93 [PubMed: 10728704]

Ehling J et al. 2014 Micro-CT imaging of tumor angiogenesis: quantitative measures describing micromorphology and vascularization Am. J. Pathol 184 431–41 [PubMed: 24262753]

Errico C, Pierre J, Pezet S, Desailly Y, Lenkei Z, Couture O and Tanter M 2015 Ultrafast ultrasound localization microscopy for deep super-resolution vascular imaging Nature 527 499–502 [PubMed: 26607546]

Fillon M 2013 Contrast-enhanced ultrasound may aid prostate cancer detection J. Natl Cancer Inst 105 444–6 [PubMed: 23492350]

Fix SM, Papadopoulou V, Velds H, Kasoji SK, Rivera JN, Borden MA, Chang S and Dayton PA 2017 Oxygen microbubbles improve tumor control after radiotherapy in a rat fibrosarcoma model IEEE Int. Ultrasonics Symp (10.1109/ULTSYM.2017.8091645)

Folkman J, Long DM and Becker FF 1963 Growth and metastasis of tumor in organ culture Cancer 16 453–67 [PubMed: 13958548]

Fujimoto JG, Pitris C, Boppart SA and Brezinski ME 2000 Optical coherence tomography: an emerging technology for biomedical imaging and optical biopsy Neoplasia 2 9–25 [PubMed: 10933065]

Gasparini G, Weidner N, Bevilacqua P, Maluta S, Palma PD, Caffo O, Barbareschi M, Boracchi P, Marubini E and Pozza F 1994 Tumor microvessel density, p53 expression, tumor size, and peritumoral lymphatic vessel invasion are relevant prognostic markers in nodenegative breast carcinoma J. Clin. Oncol 12 454–66 [PubMed: 7509851]

Gessner RC, Aylward SR and Dayton PA 2012 Mapping microvasculature with acoustic angiography yields quantifiable differences between healthy and tumor-bearing tissue volumes in a rodent model Radiology 264 733–40 [PubMed: 22771882]

Gessner RC, Frederick CB, Foster FS and Dayton PA 2013 Acoustic angiography: a new imaging modality for assessing microvasculature architecture Int. J. Biomed. Imaging 2013 936593 [PubMed: 23997762]

Jain RK 2014 Antiangiogenesis strategies revisited: from starving tumors to alleviating hypoxia Cancer Cell. 26 605–22 [PubMed: 25517747]

Jain RK, Martin JD and Stylianopoulos T 2014 The role of mechanical forces in tumor growth and therapy Annu. Rev. Biomed. Eng 16321–46

Kasoji SK, Rivera JN, Gessner RC, Chang SX and Dayton PA 2018 Early assessment of tumor response to radiation therapy using high-resolution quantitative microvascular ultrasound imaging Theranostics 8 156–68 [PubMed: 29290799]

Lee HB and Blaufox MD 1985 Blood volume in the rat J. Nucl. Med 25 72–6

Li CY, Shan S, Huang Q, Braun RD, Lanzen J, Hu K, Lin P and Dewhirst MW 2000 Initial stages of tumor cell-induced angiogenesis: evaluation via skin window chambers in rodent models J. Natl Cancer Inst 92 143–47 [PubMed: 10639516]

Lin F, Tsuruta JK, Rojas JD and Dayton PA 2017 Optimizing sensitivity of ultrasound contrast-enhanced super-resolution imaging by tailoring size distribution of microbubble contrast agent Ultrasound Med. Biol 43 2488–93 [PubMed: 28668636]

Lindsey BD, Rojas JD, Member S, Martin KH, Member S, Shelton SE, Member S and Dayton PA 2014 Acoustic characterization of contrast-to-tissue ratio and axial resolution for dual-frequency contrast-specific acoustic angiography imaging 61 1668–87

Lixia L, Jianhui L, Aimin Z, Tao M, Ping W and Bin L 2016 Comparison of application value between CEUS and conventional ultrasound in preoperative and staging diagnosis of cervical cancer Biomed. Res 27 553–6

Maresca D, Skachkov I, Renaud G, Jansen K, Van Soest G, De Jong N and Van der Steen A F W 2014 Imaging microvasculature with contrast-enhanced ultraharmonic ultrasound Ultrasound Med. Biol 40 1318–28 [PubMed: 24613639]

Mohanty K, Blackwell J, Egan T and Muller M 2017 Characterization of the lung parenchyma using ultrasound multiple scattering Ultrasound Med. Biol 43 993–1003 [PubMed: 28318888]

Mohanty K, Blackwell J, Masuodi SB, Ali MH, Egan T and Muller M 2018 1Dimensional quantitative micro-architecture mapping of multiple scattering media using backscattering of ultrasound in the near-field: application to nodule imaging in the lungs Appl. Phys. Lett 43 993–1003

Nagy JA, Chang SH, Dvorak AM and Dvorak HF 2009 Why are tumour blood vessels abnormal and why is it important to know? Br. J. Cancer 100 865–9 [PubMed: 19240721]

Nico B, Benagiano V, Mangieri D, Maruotti N, Vacca A and Ribatti D 2008 Evaluation of microvascular density in tumors: pro and contra Histol. Histopathol 23 601–7 [PubMed: 18283645]

Otsu N 1979 A threshold selection method from gray-level histograms IEEE Trans. Syst. Man Cybern 9 62–6

Page JH, Jones IP, Schriemer HP, Cowan ML, Sheng P and Weitz DA 1999 Diffusive transport of acoustic waves in stronogly scattering media Physica B 263–4 37–9

Page JH, Schriemer HP, Jones IP, Sheng P and Weitz DA 1997 Classical wave propagation in strongly scattering media Physica A 241 64–71

Phillips PJ 2001 Contrast pulse sequences (CPS): imaging nonlinear microbubbles 2001 IEEE Ultrasonics Symp. Proc. An Int. Symp. (Cat. No.01CH37263) (IEEE) vol 2 pp 1739–45

Provost J, Papadacci C, Demene C, Gennisson JL, Tanter M and Pernot M 2015 3D ultrafast doppler imaging applied to the noninvasive mapping of blood vessels *in vivo* IEEE Trans. Ultrason. Ferroelectr. Freq. Control 62 1467–72 [PubMed: 26276956]

Setola SV, Catalano O, Sandomenico F and Siani A 2007 Contrast-enhanced sonography of the kidney Abdominal Imaging 32 21–8 [PubMed: 17420958]

Sever AR, Mills P, Jones SE, Cox K, Weeks J, Fish D and Jones PA 2011 Preoperative sentinel node identification with ultrasound using microbubbles in patients with breast cancer Am. J. Roentgenol 196 251–6 [PubMed: 21257873]

Shelton SE, Lee YZ, Lee M, Cherin E, Foster FS, Aylward SR and Dayton PA 2015 Quantification of microvascular tortuosity during tumor evolution using acoustic angio Ultrasound Med. Biol 41 1896–904 [PubMed: 25858001]

Shelton SE, Lindsey BD, Dayton PA and Lee YZ 2017 First-in-human study of acoustic angiography in the breast and peripheral vasculature Ultrasound Med. Biol 43 2939–46 [PubMed: 28982628]

Shelton SE, Lindsey BD, Tsuruta JK, Foster FS and Dayton PA 2016 Molecular acoustic angiography: a new technique for high-resolution superharmonic ultrasound molecular imaging Ultrasound Med. Biol 42 769–81 [PubMed: 26678155]

Simpson DH, Chin CT and Burns PN 1999 Pulse inversion Doppler: a new method for detecting nonlinear echoes from microbubble contrast agents—ultrasonics, ferroelectrics and frequency control, IEEE Transactions on Pulse 46 372–82

Sirsi SR et al. 2012 Contrast ultrasound imaging for identification of early responder tumor models to anti-angiogenic therapy Ultrasound Med. Biol 38 1019–29 [PubMed: 22425376]

Snoeks TJA, Löwik CWGM and Kaijzel EL 2010 'In vivo' optical approaches to angiogenesis imaging Angiogenesis 13 135–47 [PubMed: 20449766]

Tourin A, Derode A, Peyre A and Fink M 2000 Transport parameters for an ultrasonic pulsed wave propagating in a multiple scattering medium J. Acoust. Soc. Am 108 503 [PubMed: 10955614]

Uffen MP, Krijnen MR, Hoogendoorn RJ, Strijkers GJ, Everts V, Wuisman PI and Smit TH 2008 Tissue identification with micro-magnetic resonance imaging in a caprine spinal fusion model Eur. Spine J 17 1006–11 [PubMed: 18512084]

Vakoc BJ, Fukumura D, Jain RK and Bouma BE 2012 Cancer imaging by optical coherence tomography: Preclinical progress and clinical potential Nat. Rev. Cancer 12 363–8 [PubMed: 22475930]

Van Der Bij S, Schaake E, Koffijberg H, Burgers JA, De Mol BAJM and Moons KGM 2011 Markers for the non-invasive diagnosis of mesothelioma: a systematic review Br. J. Cancer 104 1325–33 [PubMed: 21448170]

Weidner N, Folkman J, Pozza F, Bevilacqua P, Allred EN, Moore DH, Meli S and Gasparini G 1992 Tumor angiogenesis: a new significant and independent prognostic indicator in early-stage breast carcinoma J. Natl Cancer Inst 84 1875–87 [PubMed: 1281237]

Weidner N, Semple JP, Welch WR and Folkman J 1991 Tumor angiogenesis and metastasis—correlation in invasive breast carcinoma New Engl. J. Med 324 1–8

Yun S, Tearney G, de Boer J, Iftimia N and Bouma B 2003 High-speed optical frequency-domain imaging Opt. Express 11 2953 [PubMed: 19471415]

Zhang ZQ, Jones IP, Schriemer HP, Page JH, Weitz DA and Sheng P 1999 Wave transport in random media: the ballistic to diffusive transition Phys. Rev. E 60 4843–50

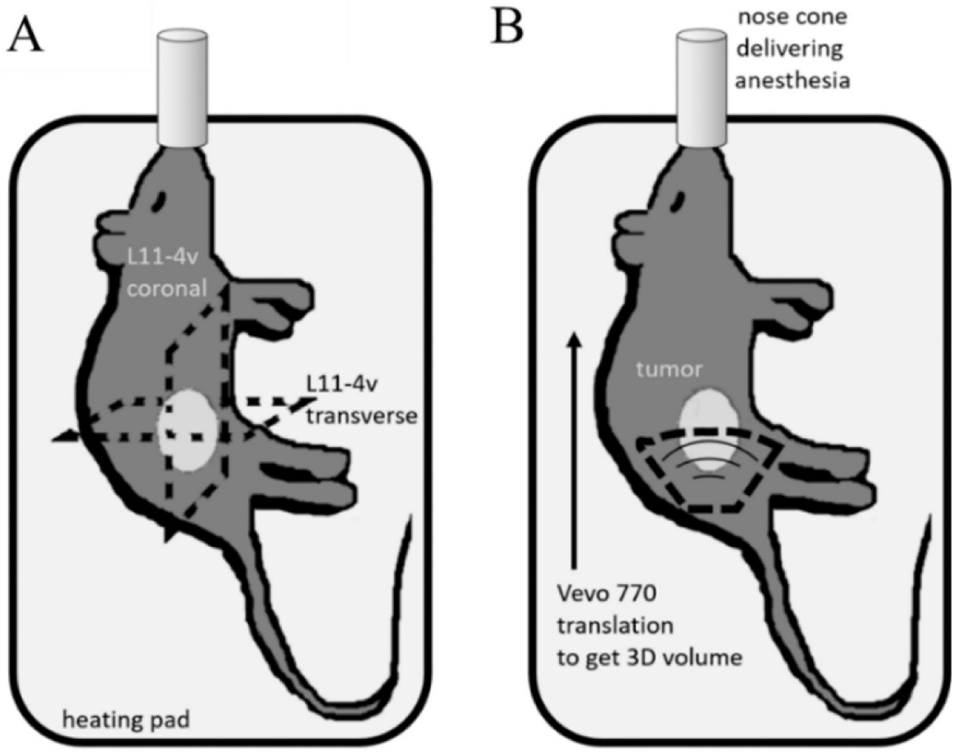

Figure 1.

Schematic of the experimental setup used for *in vivo* imaging, showing the orientations of (A) the two perpendicular planes acquired using the Verasonics for the inter-element response matrix (IRM) and (B) the B-mode and AA volumetric acquisitions using the Vevo 770.

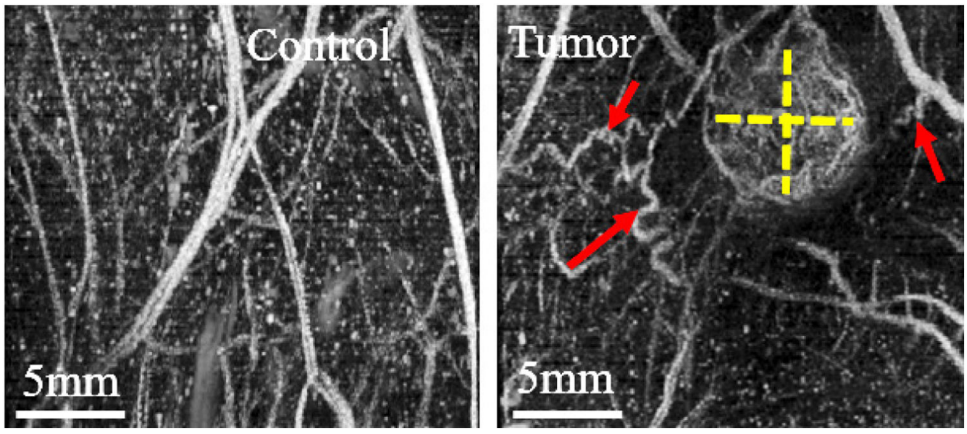

Figure 2.

Example of AA maximum intensity projections of control (left) and tumor-bearing regions (right, tumor size denoted with dashed yellow lines) in a rat fibrosarcoma model. Angiogenesis is clearly seen in the form of tortuous vessels (red arrows) around the periphery of the tumor and high vascular density (VD) in the tumor (more enhanced due to higher contrast agent perfusion). In contrast, control vasculature is generally more linear and directional, as shown.

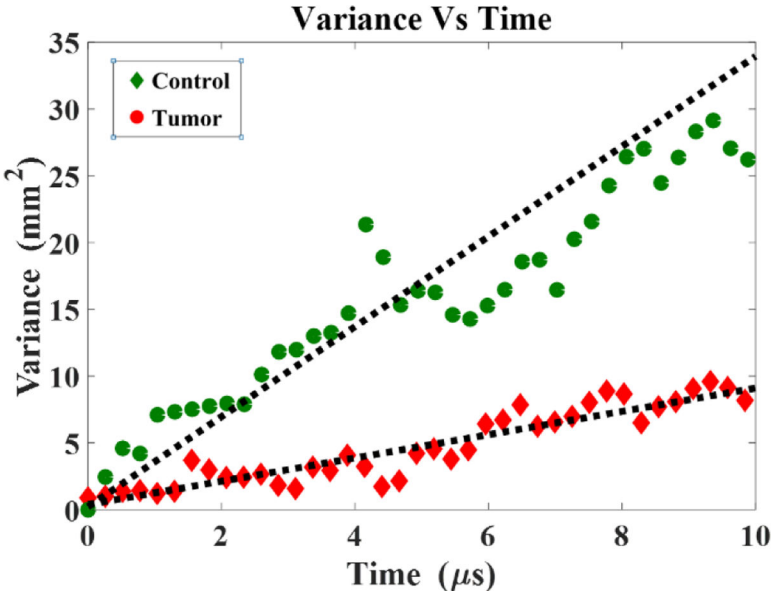

Figure 3.
Comparison of variance time evolution data for a Control and tumor case (Indicative of overall trend).

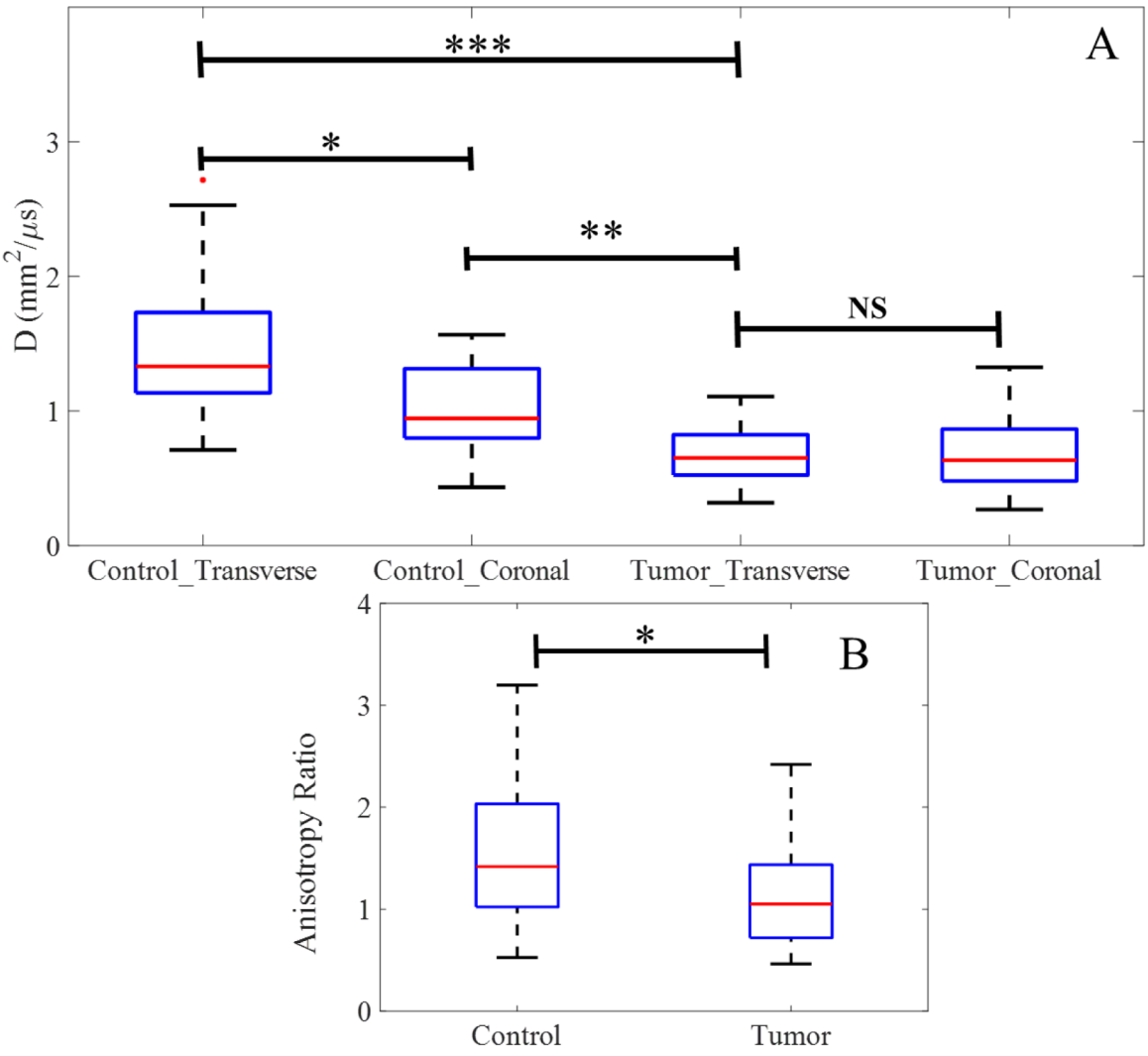

Figure 4.

(A) Comparison of the diffusion constant *D* measured along both perpendicular orientations for control and tumor, (B) and the resulting anisotropy ratios of the averaged *D* values.

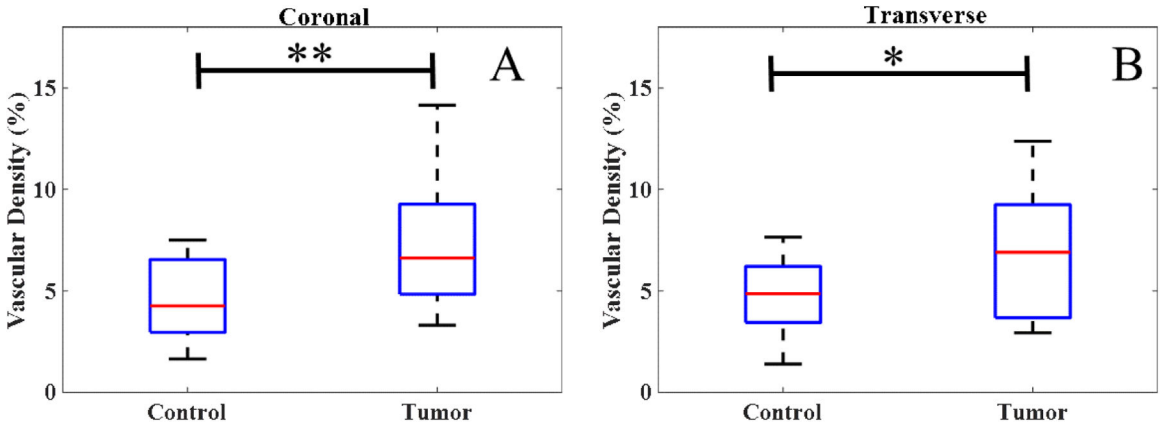

Figure 5.

VD was found significantly higher for tumors compared to controls, in both the coronal (A) and transverse (B) slices corresponding to the IRM acquisitions.